WATER RESOURCES RESEARCH, VOL. 30, NO. 9, PAGES 2547–2563, SEPTEMBER 1994

Retardation of sorbing solutes in fractured media

Christoph Wels and Leslie Smith
Department of Geological Sciences, University of British Columbia, Vancouver, Canada

Abstract. Sorption of a reactive solute during transport in a fractured geologic medium is analyzed under the assumption that within each fracture, retardation varies in proportion to the product of a surface distribution coefficient and the specific surface area of the fracture (i.e., its surface area–to-volume ratio). This approach is analogous to the K_D model commonly adopted for granular porous media. Numerical migration experiments in discrete fracture networks show that at the plume scale, retardation is both nonuniform and anisotropic. Different segments of the plume, or equivalently different breakthrough fractions at a downstream boundary, are retarded to a different degree. The degree to which various breakthrough fractions are retarded varies as a function of the orientation of the mean hydraulic gradient relative to the orientation of the fracture sets. This variation can be described in the form of a retardation ellipse. The mean arrival time is the only breakthrough fraction that is consistently described by a uniform, isotropic retardation factor. The degree of nonuniformity and anisotropy in the retardation factor is controlled largely by the difference in the mean apertures of each fracture set, the standard deviation in fracture aperture, and the orientation of the fracture sets relative to the mean hydraulic gradient. A larger variability in fracture aperture, or in the orientation of fractures within each set, promotes nonuniform retardation while reducing the degree of anisotropy in the retardation factor. Our results suggest that a transport model based on the conventional advection-dispersion equation, using a uniform retardation factor, may be conceptually incorrect, even for a dense fracture network. While the effects of nonuniform retardation modify the dispersive flux in a way that could be described by "effective" dispersion coefficients, it is our opinion that a model formulation is needed that clearly separates chemical effects from those due to hydrodynamic dispersion.

Introduction

Several countries, including Canada, France, and Sweden, are currently assessing the concept of permanent storage of high-level nuclear fuel wastes in crystalline rock. The primary pathway for solute transport is likely to be through a network of hydraulically connected fractures. Any interaction between the dissolved solutes and the fracture walls will result in the retardation of that solute and, hence, delay its arrival at the biosphere.

Based on laboratory migration experiments of radionuclides in a single fracture, Neretnieks and coworkers proposed two types of retardation mechanisms [*Neretnieks et al.*, 1982]: (1) surface sorption at the fracture walls and (2) diffusion into and bulk sorption in the rock matrix. Both types of sorption reactions are assumed to be fast, reversible processes which can be modeled using distribution coefficients obtained by equilibrating solutions containing the radionuclides of interest with the rock surface or rock matrix, respectively [e.g., *Neretnieks et al.*, 1982; *Vandergraaf et al.*, 1988]. Which of the two sorption mechanisms dominates depends, among other factors, on the porosity of the matrix, flow rates in the fractures, diffusion coefficients, and the timescale of interest. There is a large potential for bulk sorption due to the large volumes of rock matrix available relative to fracture surfaces [*Neretnieks*, 1983]. However, rates of diffusion into the rock matrix are generally much lower than flow rates within an open fracture. Generally speaking, surface sorption may prevail at small timescales, whereas bulk sorption may be dominant at large (geological) timescales.

In this paper we focus on retardation of a solute due to surface sorption on the fracture walls; matrix diffusion and bulk sorption in the rock matrix are ignored for simplicity. The first model of surface retardation was formulated by *Burkholder* [1976] for the case of a single fault and adopted to a fracture plane by *Freeze and Cherry* [1979]. According to this model the velocity of a sorbing solute is reduced by a constant retardation factor given by

$$R = 1 + \frac{SA}{V} K_a \tag{1}$$

Thus retardation varies in proportion to a surface distribution coefficient, K_a, and the surface area-to-volume ratio of the fracture (SA/V). The determination of the surface area–to-volume ratio of a fracture is difficult in a field setting. A pragmatic approach is to assume two planar, reactive fracture surfaces in an open fracture of aperture b so that the retardation equation becomes [*Freeze and Cherry*, 1979]

$$R = 1 + \frac{2}{b} K_a \tag{2}$$

Equation (2) indicates that retardation decreases with an increase in fracture aperture. Note that this behavior follows

Paper number 94WR01128.
0043-1397/94/94WR-01128$05.00

from the surface area–to-volume ratio of a fracture, indicating how much fracture surface area is available for sorption relative to the fluid volume containing the solute. It is not related to the fact that fluid and solutes typically travel faster in wider fractures; the sorption reaction is assumed to be sufficiently fast to be independent of the residence time in a fracture.

This sorption model has been used to describe breakthrough curves of sorbing solutes in machined fractures [*Vandergraaf et al.*, 1988], natural fractures in laboratory experiments [e.g., *Neretnieks et al.*, 1982; *Vandergraaf and Drew*, 1991], and field experiments [e.g., *Abelin et al.*, 1985]. Numerical migration experiments by *Moreno et al.* [1988] suggested that a similar surface retardation factor could be written for a fracture with variable aperture. They found that for the case of a distributed aperture the mean aperture simply replaces the constant aperture, b, in the formulation of R.

To our knowledge, no laboratory or field experiments have yet been performed to evaluate the suitability of an analogous retardation factor at the scale of a fracture network. However, by analogy to the case of a single fracture with variable aperture, one may postulate that the retardation factor in a fracture network is proportional to the average of the surface area–to-volume ratios of all fractures in the network. Henceforth, we refer to this medium property simply as the specific surface area of the fractured medium.

Recently, *Dverstorp et al.* [1992] used numerical migration experiments to study the influence of variable fracture aperture on retardation in sparse fracture networks. The breakthrough curves at a downstream boundary were analyzed with a one-dimensional advection-dispersion equation using a surface retardation factor based on the specific surface area. For a large standard deviation in the aperture distribution, the retardation of the median arrival time was found to be consistently lower than predicted by the retardation model based on a retardation factor using the (known) specific surface area of the network. Based on the observed R the authors calculated effective specific surface areas for the center of mass (median arrival). *Dverstorp et al.* [1992] concluded that flow channeling significantly reduced the effective values of specific surface area experienced by the solute plume compared to the average value of the fractured medium.

However, is the use of a constant retardation factor at the network scale, either based on the average medium value or an effective value of specific surface area, conceptually correct? In other words, can retardation of a sorbing solute plume in a fracture network be considered uniform? First insights can be gained by drawing comparisons to retardation in heterogeneous porous media. Stochastic analyses of reactive solute movement in heterogeneous porous media have shown that spatial variability in the retardation factor may delay the breakthrough, that is, produce a greater effective field-scale retardation factor than expected from any average of the local retardation factors [e.g., *Cvetkovic and Shapiro*, 1990]. Furthermore, negative cross correlation between the local fluid velocity and the local retardation factor may produce enhanced dispersion of the retarded solute plume [e.g., *Garabedian et al.*, 1988; *Valocchi*, 1989]. Recently, *Bellin et al.* [1993] developed an analytical solution for the spatial variance of a solute plume in a physically and chemically heterogeneous porous medium. Their results suggest that chemical heterogeneity enhances longitudinal spreading of the retarded solute plume but has little effect on transverse spreading. Numerical migration experiments by *Bosma et al.* [1993] showed that longitudinal dispersion of a solute plume may be reduced for a positive correlation between sorption coefficient and hydraulic conductivity, relative to the case of negative or no correlation.

Fractured media are often extremely heterogeneous with respect to fracture aperture which influences the local retardation factor (see equation (2)). Direct observations on cores [e.g., *Snow*, 1970] as well as hydraulic measurements [e.g., *Raven*, 1986] have shown that fracture apertures can span several orders of magnitude in a fractured rock. Since fracture aperture influences retardation at the scale of a single fracture, local retardation factors can also be expected to vary widely in a fractured rock. In addition, there is a conceptual argument for a correlation between the retardation factor and the fluid velocity in a single fracture. The retardation model (2) states that retardation in a fracture is inversely proportional to its aperture. However, fracture aperture also strongly influences the velocity of the fluid. This nonlinear coupling of fluid velocity and local retardation may prohibit the use of a constant retardation factor at the network scale. This heterogeneity in local retardation is a direct consequence of the geometric properties of the fracture system; additional chemical heterogeneity will also occur in fractured media but has not been considered here.

In this paper we evaluate the continuum concept of a retardation equation with a constant retardation factor for a fractured medium. First we review the derivation of the continuum transport equation with retardation due to surface sorption and derive a retardation factor based on the specific surface area of a fracture network. Next, we use numerical migration experiments in discrete fracture networks to show that retardation due to surface sorption is a nonuniform and anisotropic process. Different segments of a plume, or equivalently, different breakthrough fractions at a downstream boundary, are retarded to a different degree. Hence surface sorption may either reduce or increase the dispersion of the breakthrough curve depending on the network geometry and its orientation in the flow field. We will show that only the mean arrival time is predicted accurately when using a constant retardation factor based on the specific surface area.

Retardation Models

The concept of retardation is based on experimental data which show that the partitioning of many solutes between the solid and the aqueous phase is a fast, reversible process which can be described by a linear isotherm. With the assumption of linear sorption the transport equation for a sorbing solute in a homogeneous porous medium [e.g., *Freeze and Cherry*, 1979] is given by

$$\frac{\nabla \cdot (\mathbf{D}\nabla C)}{R_f} - \frac{\nabla \cdot (C\mathbf{V})}{R_f} = \frac{\partial C}{\partial t} \tag{3a}$$

where $\mathbf{V}$ is the average linear velocity of the groundwater and $\mathbf{D}$ is the dispersion tensor. R_f is known as the retardation factor,

$$R_f = 1 + \frac{\rho_b}{\theta} K_D \tag{3b}$$

where θ and ρ_b are the porosity and the bulk density of the porous medium, respectively, and K_D is the distribution coefficient (all assumed to be constant). It is seen from (3a) that the effect of sorption is to decrease both the advective flux and the dispersive flux by a constant retardation factor, R_f.

The retardation concept may also be applied to a fractured medium where the host rock is assumed impermeable and all sorption reactions are limited to the fracture walls (surface sorption). Here, the amount of solute, S^*, sorbed to the solid in an isotherm experiment is better expressed in terms of the surface area of the sorbate. Introducing the surface distribution coefficient, K_a, we have [*Neretnieks et al.*, 1982]

$$S^* = K_a C \tag{4}$$

where the mass of solute, S^*, sorbed on the solid part of the fractured medium per unit surface area of sorbate is proportional to the solute concentration, C, in solution. K_a can be determined in static sorption experiments by exposing rock coupons containing fracture surface material to a solution containing a sorbing solute of interest [e.g., *Vandergraaf et al.*, 1988].

The transport of a reactive solute in a fractured medium of constant porosity can be described in a general form as

$$-\theta \nabla \cdot F = \theta \frac{\partial C}{\partial t} + \frac{\partial q}{\partial t} \tag{5}$$

where F is the total (advective and dispersive) flux of the solute C in a unit volume of rock, θ is the porosity, and q is the mass of solute that is transferred to the sorbate per unit volume of rock. The derivation of the surface retardation factor for a fractured medium is analogous to that for a porous medium with one important exception. We need to consider the bulk surface area, A_b, of the fractured medium in order to relate q in the transport model (5) to S^* given by the isotherm experiment (4). In the context of surface sorption in a fractured medium, q is linked to S^* via the relation

$$q = A_b S^* \tag{6}$$

where A_b is defined as the total surface area of all hydraulically connected (open) fractures per unit volume of rock. Differentiating (4) and (6) with respect to time and assuming θ and A_b are constant in space and time, the transport equation for a sorbing solute in a fractured medium simplifies to

$$-\nabla \cdot F = \left(1 + \frac{A_b}{\theta} K_a\right) \frac{\partial C}{\partial t} \tag{7}$$

The term in parentheses is a constant which we define as the surface retardation factor, $\langle R \rangle$, for the fractured medium. The angle brackets identify parameters which are used at the network scale and which need to be distinguished from equivalent parameters at the scale of a single fracture. Assuming all fractures can be approximated by parallel plates of variable length, l_n, and aperture, b_n, and further assuming a constant depth, D, for all fractures that is much greater than b_n (i.e., a two-dimensional problem), the bulk surface area and porosity can be written for a unit volume, V, of fractured rock with N fractures as

$$A_b = \frac{\sum_{n=1}^{N} 2 l_n D}{V} \tag{8}$$

with dimensions $[L^2]/[L^3]$ and

$$\theta = \frac{\sum_{n=1}^{N} l_n b_n D}{V} \tag{9}$$

with dimensions $[L^3]/[L^3]$. We define the ratio of A_b over θ as the specific surface area, $\langle a \rangle$, of the fractured medium,

$$\frac{A_b}{\theta} = \langle a \rangle = \frac{2 \sum_{n=1}^{N} l_n}{\sum_{n=1}^{N} l_n b_n} \tag{10}$$

We emphasize that $\langle a \rangle$ is defined as the ratio of the surface area of (open) fractures to the fracture volume, and not to the total volume, V, of the fractured rock. Substituting (10) into (7), the surface retardation factor, $\langle R \rangle$, for a fractured medium becomes

$$\langle R \rangle = 1 + \langle a \rangle K_a \tag{11}$$

Note that this continuum retardation equation (11) for a fractured medium is consistent with the retardation equation (2) given earlier for a single fracture. If the fractured medium consists of a single fracture, $\langle a \rangle$ simply reduces to the surface area–to-volume ratio of this fracture, that is, two over the fracture aperture.

The specific surface area, $\langle a \rangle$, is calculated from all fractures present in a representative elementary volume (REV) of the fractured medium. *Dverstorp et al.* [1992] have termed $\langle a \rangle$ the "geometric estimate" of the specific surface area. Similarly, $\langle R \rangle$ in (11) may also be referred to as the geometric retardation factor. The use of $\langle a \rangle$ in the continuum retardation equation is justified only if the solute plume encounters a representative (unbiased) sample of fractures along its flow path. Any significant channeling (i.e., a bias toward transport in wider fractures) that involves the entire solute plume should yield a reduction in the observed ("effective") value of specific surface area and consequently the retardation factor.

There is considerable practical advantage in replacing the explicit formulation of $\langle a \rangle$ (equation (10)) by an approximation involving only the mean values of fracture length and aperture as well as fracture density. Consider a network of two fracture sets with N^i and N^j fractures, respectively. Assuming that the fracture aperture and fracture length of each fracture set are independent random variables given by a probability distribution with mean values l_m^i, b_m^i for

fracture set I, and l_m^j, b_m^j for fracture set J, respectively, the specific surface area can be approximated as

$$\langle a \rangle = \frac{2N^i l_m^i + 2N^j l_m^j}{N^i l_m^i b_m^i + N^j l_m^j b_m^j} \tag{12}$$

It should be kept in mind that the independence of the fracture length and aperture is a crucial assumption in identifying this approximation for $\langle a \rangle$. This assumption may or may not be satisfied in fractured geologic material depending on the genesis of the fracture network [e.g., *Chernyshev and Dearman*, 1991]. Equation (12) is easily rewritten in terms of fracture density. The fracture density, γ, of a fracture set can be expressed by the ratio of the total number of fractures in this set per volume of rock (e.g., $\gamma^i = N^i/V$). Substituting the product of the respective fracture density and V for total numbers of fractures of each set in (12), V cancels and we have

$$\langle a \rangle = \frac{2\gamma^i l_m^i + 2\gamma^j l_m^j}{\gamma^i l_m^i b_m^i + \gamma^j l_m^j b_m^j} \tag{13}$$

This formulation of specific surface area $\langle a \rangle$ is readily extended to three dimensions by assuming a probability distribution for fracture depth (instead of a constant D). This extension would introduce the mean fracture depth of each fracture set into (13).

In the following we consider a few special cases for which the specific surface area $\langle a \rangle$ of a network with two fracture sets can be further simplified. These special cases will be explored in our migration experiments to be discussed later. If the two fracture sets have a common mean aperture b_m, that is, b_m^i is equal to b_m^j, we have

$$\langle a \rangle = \frac{2(\gamma^i l_m^i + \gamma^j l_m^j)}{b_m(\gamma^i l_m^i + \gamma^j l_m^j)} = \frac{2}{b_m} \tag{14}$$

For this special case, $\langle a \rangle$ can be estimated directly from the common mean aperture. The specific surface area is independent of the mean fracture length and the total number of fractures of the two fracture sets, respectively. In contrast, if we assume that the two fracture sets have a common mean fracture length l_m, that is, l_m^i is equal to l_m^j, we have

$$\langle a \rangle = \frac{2l_m(\gamma^i + \gamma^j)}{l_m(\gamma^i b_m^i + \gamma^j b_m^j)} = \frac{2(\gamma^i + \gamma^j)}{(\gamma^i b_m^i + \gamma^j b_m^j)} \tag{15}$$

Here $\langle a \rangle$ is given by twice the inverse average of the two mean aperture values weighted by the relative fracture densities of the two fracture sets. For a fracture network composed of two fracture sets with equal fracture density and a common mean fracture length l_m, the specific surface area is given by

$$\langle a \rangle = \frac{4}{b_m^i + b_m^j} \tag{16}$$

that is, twice the inverse average of the two aperture means.

In summary, the transport equation for a sorbing solute in a fractured medium is given as

$$-\nabla \cdot F = (1 + \langle a \rangle K_a) \frac{\partial C}{\partial t} \tag{17}$$

where the term in parentheses is defined as the (geometric) surface retardation factor, $\langle R \rangle$. For a fracture network composed of two fracture sets the specific surface area is given by the general formulation (13). The above transport equation applies to a fractured medium that satisfies the following assumptions: (1) fracture planes are open and can be approximated by parallel plates, (2) fracture length and fracture aperture are statistically independent, (3) no significant channeling (biased sampling of wide fractures) of the entire solute plume occurs at the scale of the REV, and (4) a uniform and isotropic retardation factor exists at the network scale. The last assumption is perhaps the most interesting. It implies that at the continuum scale the entire flux of the solute (advection and dispersion) has to be reduced equally by sorption. In addition, this retardation of the solute plume has to be independent of the direction of the hydraulic gradient. Only then is the use of a constant retardation factor $\langle R \rangle$ justified. Most of the discussion in this paper will focus on assumption 4.

A transport experiment in the field or laboratory is needed to test the validity of these assumptions. For this purpose the retardation factor would be determined experimentally using the retardation equation for a fractured medium,

$$\langle R \rangle = \frac{\langle v \rangle}{\langle v_r \rangle} = 1 + \langle a \rangle K_a \tag{18}$$

where $\langle v \rangle$ and $\langle v_r \rangle$ are the average linear velocities of the groundwater (or a conservative solute) and a reactive solute, respectively, in the fractured medium. Commonly, retardation factors are determined from breakthrough curves (BTC) in tracer experiments. *Brusseau and Rao* [1989] pointed out that the mean arrival time is the correct reference point to estimate a retardation factor. This method yields good estimates of $\langle R \rangle$ even in the case of nonideal (nonequilibrium) sorption behavior because the first time moment is independent of enhanced spreading due to kinetic limitations in the sorption behavior [*Brusseau and Rao*, 1989, and references therein]. Although (18) provides a way to estimate $\langle R \rangle$, it does not test whether the same retardation applies to all segments of the solute plume traveling through the medium. Assuming that molecular diffusion does not contribute significantly to dispersion, a more general retardation equation can be written,

$$\langle R \rangle_{\text{ref}} = \frac{\langle v \rangle_{\text{ref}}}{\langle v_r \rangle_{\text{ref}}} = 1 + \langle a \rangle K_a \tag{19}$$

where the index "ref" indicates any reference point of the solute plume (or equivalently any reference point on a BTC at a downstream boundary). The general retardation equation (19) above is satisfied if the entire breakthrough curve is retarded equally, that is, shifted by a constant $\langle R \rangle$. This relation implies that surface sorption reduces the advective and dispersive flux by a constant $\langle R \rangle$ as assumed for the reactive transport equation (17). The numerical migration experiments described below will demonstrate that this assumption is not generally justified.

Numerical Migration Experiments: Design and Choice of Parameters

The fractured medium in our migration experiments is represented by two-dimensional fracture networks gener-

ated stochastically from a set of fracture system statistics [*Clemo*, 1994]. The numerical model generates a network of open fractures by randomly locating fracture midpoints using a uniform distribution. Fracture orientations are normally distributed, and fracture length is specified by a negative exponential probability distribution. Fracture aperture is lognormally distributed and does not vary along the length of a fracture. These stochastic input parameters are all independent. The networks studied here consist of two sets of fractures. Each set is specified by scan line density (γ_s), mean length (l_m), mean aperture (b_m), and the standard deviation of aperture in $\log_{10}$ space (σ). Scan line density is the expected number of intersections of the fractures in a set with a line of unit length that is normal to the mean orientation of the set.

Flow and transport are simulated using a modified version of the finite difference model DISCRETE [*Clemo*, 1994]. The fracture segments between fracture intersections have a constant flow. The flow is related to the hydraulic head drop between intersections by

$$Q = \frac{\rho g}{12\mu} b^3 \frac{\Delta h}{\Delta l} \tag{20}$$

where Q is the volumetric flow in a fracture segment of unit depth, Δh is the head drop between the intersections, and Δl is the distance between the intersections. Conservation of mass at the intersections results in a set of linear equations that describe the flow within the domain.

Transport is modeled using a particle-tracking routine. For any single network realization, two runs are performed: (1) transport of a nonsorbing ("conservative") solute and (2) transport of a reactive solute sorbing to the fracture walls (equilibrium surface sorption). Nonreactive particles travel from intersection to intersection according to the residence time of the fluid, τ, in a fracture segment given by

$$\tau = b\Delta l/Q \tag{21}$$

Stream tube routing is implemented at the fracture intersections. Surface sorption is modeled by increasing the residence times of all fracture segments by their respective surface retardation factor, R, as defined by the retardation equation for a single fracture (equation (2)). This transport routine assumes plug flow, that is, dispersion at the single fracture scale is negligible compared to dispersion at the network scale [e.g., *Hull et al.*, 1987]. This assumption is a reasonable approximation for the vast majority of fracture segments under the flow conditions studied in our migration experiments.

The flow domain and the boundary conditions are chosen to mimic the conditions of a tracer experiment at the near-field scale. The flow domain is 10 m by 10 m with constant head boundaries on the left and right and no-flow boundaries at the top and bottom (Figure 1). The magnitude of the head gradient between the constant head boundaries were set to 0.01. However, the magnitude of the global hydraulic gradient does not influence the retardation behavior studied here. Several migration experiments in dense networks (see reference geometry below) were rerun on a larger flow domain (20 m by 20 m) with identical boundary conditions as those shown in Figure 1. No significant differences in the retardation behavior were observed, suggesting

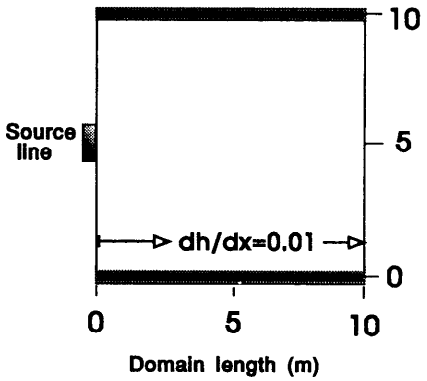

Figure 1. Flow domain, boundary conditions, and the source zone used in the simulations. No-flow boundaries are imposed at the top and bottom of the model domain.

that a domain size of 10 m by 10 m is sufficiently large to study a representative retardation behavior in the dense networks considered here.

The solute is introduced as an instantaneous pulse along a line source of 1 m length in the center of the left (upgradient) boundary (Figure 1). The line source is centered on the inflow boundary so as to minimize the influence of the no-flow boundaries on the spreading of the solute plume. A source length of 1 m was sufficiently large to provide good access (approximately four to six injection nodes) to the dense fracture networks studied here. Transport calculations are not performed in individual network realizations if (1) no fracture intersects the source area or (2) the combined flow rate for all intersecting fractures is less than 10% of the flow rate across the domain. This filter ensures that the particles are not trapped in close proximity of the source due to poor connection of the source line to the network. Sensitivity analyses indicated that although this filter artificially reduces the variance in the transport results (in particular for the sparse network in scenario 2), it does not influence the general pattern of behavior we observed. Transport of a single particle is completed when it reaches the downstream (right) boundary. Its total transport time is given as the sum of the fracture residence times determined during transport through the network. The distribution of total transport times for a large number of particles constitutes the breakthrough curve (BTC) for a given transport simulation.

The particle-tracking technique requires the use of a sufficiently large number of particles so that the transport characteristics do not change with a further increase in the number of particles. In the networks studied here, 5000 particles are sufficient to characterize the reactive transport behavior. No significant deviations in transport results were obtained in comparative runs with up to 50,000 particles. Four retardation factors, $\langle R\rangle_5$, $\langle R\rangle_{50}$, $\langle R\rangle_m$, and $\langle R\rangle_{95}$ are determined for each network realization by comparing the arrival times of four reference mass breakthrough fractions, T_5, T_{50}, T_m, and T_{95} in a conservative and reactive transport run. These reference points (5%, 50%, mean, and 95% mass breakthrough fraction) have been chosen to compare retardation of the leading edge, the center, and the tail of the solute plume. Note that the solute breakthrough curves in most fractured media are skewed to the right, so

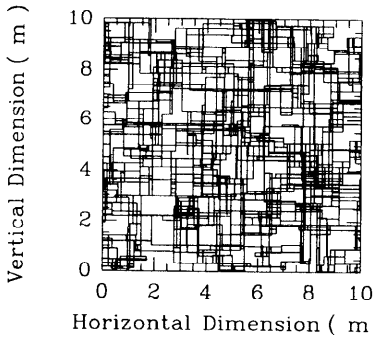

Figure 2. Single realization of a fracture network representing the reference geometry used in scenarios 1 and 3–4. Only the hydraulically connected network is shown. See Table 1 for fracture statistics.

that the mean arrival time is later than the arrival time of the center of mass (i.e., $T_m > T_{50}$).

In accord with the general retardation equation (19) a continuum transport equation with a constant retardation factor can be formulated if these four $\langle R \rangle_{ref}$ are equal (assuming no diffusion into the rock matrix). In this case of uniform retardation, the four $\langle R \rangle_{ref}$ may either approximate the (known) geometric retardation factor $\langle R \rangle$ (equation (11)) or converge to an (unknown) effective retardation factor. However, if the four $\langle R \rangle_{ref}$ differ significantly, the retardation process is considered nonuniform and a constant retardation factor is not applicable. An alternative interpretation of the experiments would be to fit an advection-dispersion model to the BTC of the sorbing solute [e.g., *Dverstorp et al.*, 1992]. In this procedure, nonuniform retardation could potentially be accounted for by fitting an effective dispersion coefficient to a retardation run. As discussed in a later section, from a conceptual viewpoint, we prefer to separate hydrodynamic dispersion from that due to chemical interaction.

Transport properties (nonreactive and reactive) vary considerably among individual realizations of a given fracture network description. This variability results from differences in the arrangement and connectivity of fractures that are possible within the stochastic network description. Trial runs with up to 500 Monte Carlo realizations showed that stable average values for T_{ref} and $\langle R \rangle_{ref}$ were obtained for ~100 Monte Carlo realizations of a given fracture network description. All results presented here are based on 250 Monte Carlo realizations.

The extent of retardation due to surface sorption depends on the type of network studied. In this paper, we study primarily dense fracture networks in which a continuum approximation to reactive transport would appear to be most promising. Figure 2 shows an example of a fracture network with the reference geometry used in the majority of the migration experiments. This reference geometry consists of two orthogonal fracture sets each with a mean length of 1 m and a scan line density of six fractures per meter. This combination of fracture length and scan line density represents well-connected and dense networks (10–20 intersections per square meter).

Fracture length, fracture density, and fracture aperture all influence specific surface area (see equation (13)) and presumably retardation. However, in this paper we consider primarily the influence of fracture aperture on retardation. Therefore all networks studied here are composed of two fracture sets with equal mean fracture length, l_m, of 1 m and equal fracture density. In this way, specific surface area and the geometric retardation factor can be estimated directly from the mean aperture of the two sets (equation (16)).

The range of fracture apertures, b, in each fracture set is represented by a lognormal density distribution which is given (for $b > 0$) as

$$n(b) = \frac{1}{b[2\pi(\ln 10\sigma)^2]^{1/2}} \exp \frac{-(\log b - \log b_0)^2}{2\sigma^2} \quad (22)$$

and specified by two parameters, the mean ($\log b_0$) and standard deviation (σ) of aperture in log 10 space. The nontransformed value b_0 is the most probable aperture value (geometric mean) and is related to the (arithmetic) mean aperture, b_m, by

$$b_m = b_0 \exp \frac{(\ln (10)\sigma)^2}{2} \quad (23)$$

As can be seen from (23), the geometric mean, b_0, is always smaller than the arithmetic mean, b_m. Note that the specific surface area (equations (13)–(16)) is estimated based on the arithmetic mean aperture, b_m.

We study the sensitivity of retardation to the spread (or variability) in the aperture distribution by varying σ. However, the resulting aperture distributions differ considerably in shape depending on whether the geometric mean b_0 or the arithmetic mean b_m is held constant [e.g., *Tsang et al.*, 1988]. The use of a constant b_m generally gives more weight to the lower aperture values relative to that using a constant b_0. Note that for $\sigma = 0$ the aperture distribution collapses to a single aperture value ($b = b_0 = b_m$). In our sensitivity studies the arithmetic mean aperture, b_m, is held constant so that the specific surface area and the geometric retardation factor of the network remain constant.

Results of migration experiments for six types of fracture networks (scenarios) are presented in this paper. The different network parameters used for these scenarios are summarized in Table 1. Scenarios 1 and 3–4 use the dense and well-connected reference geometry of two orthogonal sets shown in Figure 2. The only parameters to be varied relate to the aperture distribution for the two sets. In the first scenario we study a fracture network where the two fracture sets are described by a common aperture distribution with a constant mean b_m equal to 80 μm (Table 1). In scenarios 3 and 4 we study a network where each fracture set has a distinct aperture distribution with b_m equal to 20 μm and 80 μm, respectively. Scenarios 3 and 4 differ in the orientation of the network with respect to the overall direction of flow (Table 1). In the remaining three scenarios we study "connectivity effects" by changing the network geometry itself. In scenario 2 we reduce the fracture density of the fracture network with common aperture distribution by half relative to the reference geometry. In the last two scenarios we study fracture networks in which the two fracture sets (with differing mean apertures) are not strictly orthogonal (scenario 5) or show no preferred mean orientation (scenario 6).

For each scenario, arrival times and $\langle R \rangle_{ref}$ are calculated repeatedly while systematically increasing σ from 0 to 0.5 in both sets. The sorption strength of the surface reaction

Table 1. Summary of Fracture Network Input Parameters Which Were Varied in the Six Transport Experiments

Scenario	Mean Fracture Aperture, μm		Fracture Orientation,* deg		Fracture Scan Line Density,† fractures per meter	
	b_m^1	b_m^2	α_1	α_2	γ_1	γ_2
1	80	80	0.0	90.0	6.0	6.0
2	80	80	0.0	90.0	3.0	3.0
3	80	20	0.0	90.0	6.0	6.0
4	80	20	90.0	0.0	6.0	6.0
			Near-Orthogonal			
5	80	20	0.0 ± 10.0 (90.0 ± 10.0	90.0 ± 10.0 0.0 ± 10.0)	6.0	6.0
			Random			
6	80	20	0.0 ± 90.0 (90.0 ± 90.0	90.0 ± 90.0 0.0 ± 90.0)	6.0	6.0

All fracture networks are composed of two sets of fractures. The mean fracture length of both sets is 1.0 m in all runs.

*Orientation of each fracture set with respect to the overall hydraulic head gradient (i.e., with respect to the horizontal); in scenarios 5 and 6 two (principal) orientations of the network were studied (see text).

†Fracture densities used for generation of the network; densities actually observed for the hydraulically connected network within the flow domain are slightly lower (by no more than 3% of the input value).

characterized by K_a is held constant in all simulations. We have chosen K_a somewhat arbitrarily ($K_a = 4 \times 10^{-3}$ m) so that the geometric retardation factor $\langle R \rangle$ is equal to 101 in the first scenario (with $\langle a \rangle = 2/b_m = 2.5 \times 10^{+4}$ m). The chosen value of K_a is within the range of K_a values measured in static sorption experiments for weakly sorbing radionuclides [e.g., *Vandergraaf and Drew*, 1991].

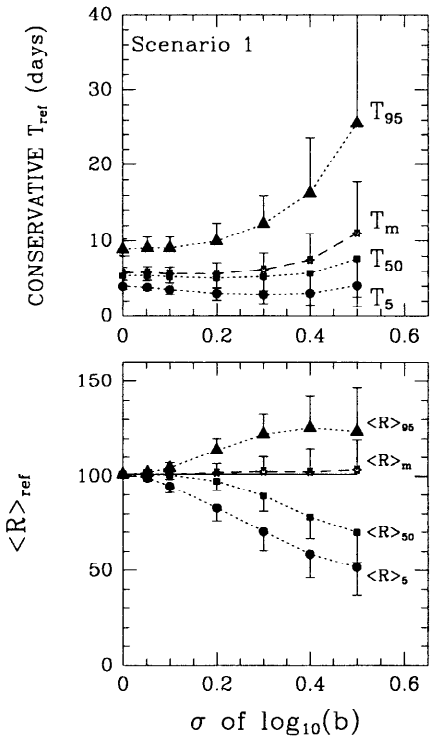

Figure 3. Transport behavior in the dense network of scenario 1. The two fracture sets have a common aperture distribution ($b_m = 80$ μm). Shown are the average values for (top) conservative arrival times T_{ref} and (bottom) retardation factors $\langle R \rangle_{ref}$. The standard deviation of these estimates is indicated by the one-sided error bars. The geometric estimate of $\langle R \rangle$ in scenario 1 is equal to 101 (solid line).

Results and Discussion

Two Orthogonal Fracture Sets With a Common Aperture Distribution

In the first scenario we study the retardation behavior in a dense fracture network where the two fracture sets are described by a common aperture distribution. Figure 3 summarizes the transport behavior of a conservative and sorbing solute in scenario 1. The upper panel shows the average arrival times, T_{ref}, of the conservative solute at the downgradient (right) boundary as a function of σ. The respective retardation factors, $\langle R \rangle_{ref}$, are shown in the lower panel. The arrival times of the sorbing solute are easily back calculated by multiplying $\langle R \rangle_{ref}$ by T_{ref}. All values are average values of 250 Monte Carlo realizations with a standard deviation indicated as one-sided error bars.

Two general observations can be made in this experiment with respect to retardation at the plume scale. First, the four $\langle R \rangle_{ref}$ are not equal except for the special case where all fractures have the same aperture ($\sigma = 0$). This behavior suggests that the concept of a single retardation factor rigorously applies only to a network composed of fractures with equal aperture. Provided there is any variability in fracture aperture ($\sigma > 0$), retardation at the plume scale cannot be considered uniform. The difference in retardation factors $\langle R \rangle_{ref}$ can be significant depending on the spread in the aperture distribution. For example, consider the fracture network in which fracture aperture varies by approximately 1 order of magnitude ($\sigma = 0.3$). In this case the 5 percentile breakthrough fraction is retarded by a factor of ~70 whereas the 95 percentile breakthrough fraction is retarded by a factor of ~120 (Figure 3).

Second, the geometric estimate of the retardation factor (here $\langle R \rangle = 101$) which is based on the specific surface area, $\langle a \rangle$, accurately predicts the retardation of the mean arrival time for the entire range of σ values considered (Figure 3). At the same time, the geometric estimate of $\langle R \rangle$ consistently overestimates retardation for breakthrough fractions ahead of the mean arrival time and underestimates retardation for breakthrough fractions arriving later than the mean arrival time (Figure 3). This systematic deviation of the observed

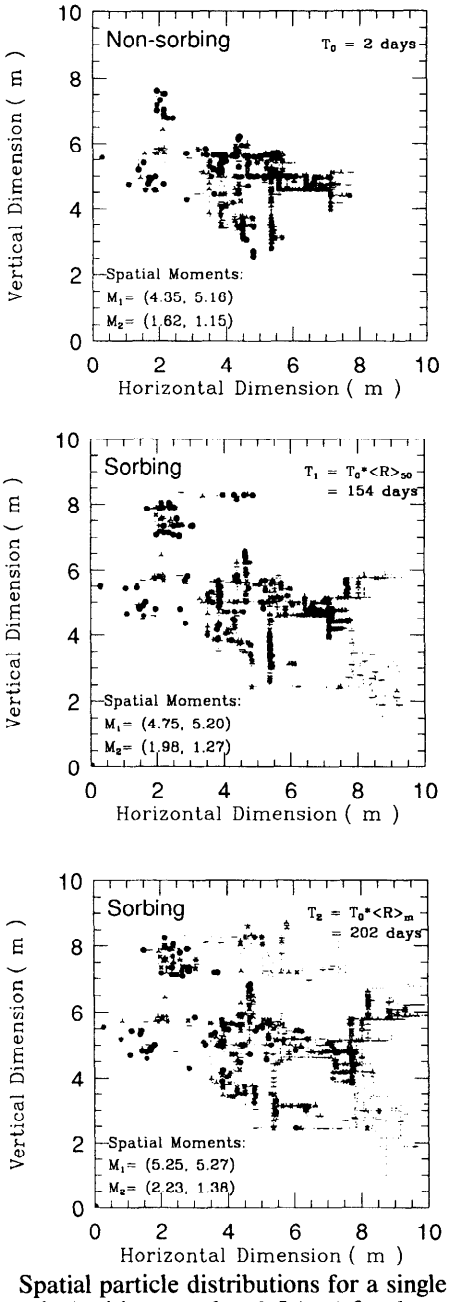

Figure 4. Spatial particle distributions for a single realization of scenario 1 with σ equal to 0.5 (top) for the conservative solute plume at T_0 = 2 days, (middle) for the sorbing solute plume at $T_1 = T_0\langle R\rangle_{50}$ = 154 days, and (bottom) for the sorbing solute plume at $T_2 = T_0\langle R\rangle_m$ = 202 days. The spatial distribution of 5000 particles was discretized in a grid of 1000 by 1000 cells. The number of particles per grid cell is indicated by the number of vertices used to draw the data point. The first (M_1) and second (M_2) spatial moments (x, y) of the respective solute plumes are shown in each panel as well.

$\langle R\rangle_{\text{ref}}$ from the geometric $\langle R\rangle$ is a result of biased "sampling" of fractures by the solute particles. For example, a fast particle representing the 5 percentile breakthrough fraction preferentially travels in fractures of wide aperture since these fractures tend to have higher flow rates (see equation (20)) and shorter residence times. It follows that the effective specific surface area experienced by a fast particle is lower than the geometric estimate of $\langle a\rangle$; hence the resulting retardation factor $\langle R\rangle_5$ is also lower than the geometric $\langle R\rangle$. Similar arguments can be made to explain the greater retardation of slow particles (e.g., $\langle R\rangle_{95}$) relative to the geometric estimate.

The mean arrival time T_m of the conservative solute is greater than the arrival time of the 50% breakthrough fraction T_{50}, indicating a BTC which is skewed to the right (Figure 3). Consistent with the above line of reasoning, the faster center of mass shows a lower $\langle R\rangle_{50}$ than the mean arrival time ($\langle R\rangle_m \sim \langle R\rangle = 101$) for all σ values greater than ~0.1 (Figure 3). Such differences cannot be confirmed in a statistical framework due to the high standard deviations in the mean values of T_{ref} as well as $\langle R\rangle_{\text{ref}}$, in particular for large values of σ. However, the trend of a lower $\langle R\rangle_{50}$ relative to $\langle R\rangle_m$ has been observed in most realizations of this scenario.

The observed differences in the values of $\langle R\rangle_{50}$ and $\langle R\rangle_m$ raise a question concerning which reference point is more appropriate for estimating the "average" retardation of a solute plume. *Brusseau and Rao* [1989] favor the use of the mean arrival time to estimate a retardation factor. They argue that T_m is a truer measure of retardation than is T_{50} because the retardation of T_m is independent of any nonequilibrium effects (kinetic limitations in the sorption reaction). As shown here, retardation of T_m is independent of any spatial heterogeneity of local retardation (nonuniform sorption) in a network of fractures (Figure 3). In principle, this allows a prediction of retardation of the mean arrival time from the specific surface area of the fractured medium (or vice versa). From a practical viewpoint, however, this reference time is influenced significantly by the tail of the BTC which can be very long and difficult to measure accurately. This dependence on the tail of the BTC makes it much more difficult to determine T_m in an experiment than the arrival time of the center of mass (T_{50}). More importantly, the strong weight that the tail of the plume gives to T_m (and subsequently $\langle R\rangle_m$) results in an estimate of plume retardation which is often not representative of the retardation of the faster "bulk" of the plume.

To illustrate this point we have plotted snapshots of the spatial distribution of the particles in a network realization of scenario 1 for the conservative run and the retardation run (Figure 4). The spatial distribution of the conservative solute plume is shown for the time T_0 equal to 2 days after pulse injection. At this time all particles are still present in the domain. This spatial distribution should be approximately reproduced by the retardation run at a time T_0 multiplied by the "average" $\langle R\rangle$. A visual comparison of the retarded plumes for times equal to 154 days ($T_1 = T_0\langle R\rangle_{50}$) and 202 days ($T_2 = T_0\langle R\rangle_m$) with the conservative plume shows that $\langle R\rangle_{50}$ is a better estimator for the retardation of the "bulk" of the plume (Figure 4). In particular, the retardation of the front of the plume is much better captured using $\langle R\rangle_{50}$. In contrast, the differences in using $\langle R\rangle_{50}$ or $\langle R\rangle_m$ for predicting the retardation of the tail of the plume are minor.

In densely fractured media, spatial moments provide a meaningful description of the spatial distribution of the solute plume; that is, the first and second moments represent the center of mass and the degree of spatial dispersion of the solute plume, respectively [*Smith et al.*, 1990]. A comparison of the first and second spatial moments of the three solute plumes (M_1 and M_2, respectively; Figure 4) confirms

the visual impression that a retardation factor estimated from T_{50} describes the spatial distribution of a reactive solute plume (both center of mass and spreading) much better than does an estimate of $\langle R \rangle$ based on T_m. Unfortunately, the geometric estimate of $\langle R \rangle$ is not a good model for $\langle R \rangle_{50}$, in particular for high σ (Figure 3).

A Continuum Model for Nonuniform Retardation?

The results of scenario 1 clearly demonstrate that even for a dense and well-connected fracture network retardation is more complicated than the conventional retardation model applied in a granular porous medium. The major difference between the K_a approach in a fractured medium and the K_D approach in a porous medium lies in the way local retardation is linked to local particle velocities. This point is best understood by considering the influence of sorption on the particle velocity distribution. In the Fickian dispersion model for a porous medium the solutes are assumed to sample randomly from a velocity distribution of which the first and second moments define the average linear velocity and the dispersion of the conservative solute, respectively [*Bear*, 1972]. In the traditional K_D approach it is assumed that the entire velocity distribution is shifted by a constant retardation factor for a sorbing solute. In this way the average linear velocity and the dispersion coefficient are both reduced by this retardation factor (equation (3a)). Because it is not possible to measure the velocity distribution, this assumption can only be tested at the continuum scale using an equivalent form of the general retardation equation (19).

In the K_a approach developed here, we assume a priori a relationship between the velocity of a conservative solute and a sorbing solute at the scale of a single fracture in the form of (2). In principle, the reactive particle velocity distribution is shifted by a constant factor only if aperture is constant for all fractures of the network, that is, σ is equal to 0. The use of discrete fracture networks allows us to calculate the distribution of local particle velocities in the network. Figure 5 shows such particle velocity distributions for a conservative and a retardation run observed in a single network realization of scenario 1. As expected, for σ equal to zero the entire velocity distribution for reactive particles is shifted toward a lower average particle velocity but the spread in particle velocities is constant (Figure 5 (top)). In contrast, for a fracture network with variable aperture (e.g., $\sigma = 0.5$) the velocity distribution is not simply shifted by a constant factor; instead the mean as well as the standard deviation of the reactive particle velocity distribution is changed relative to the conservative particle (or fluid) velocity distribution (Figure 5 (bottom)). This perturbation in the velocity distribution arises because fracture aperture influences not only the local retardation factor but also the fluid velocity itself (see (20)). In scenario 1 this coupling of fluid velocity and retardation via fracture aperture gives rise to a substantial increase in the spread of the velocity distribution when introducing retardation (Figure 5 (bottom)). This increased spread in the particle velocities explains the enhanced dispersion of the retarded solute plume relative to the plume of a nonsorbing solute (Figure 4). Dispersion of the retarded solute plume remains unchanged only in a network with no spatial variability in local retardation (uniform retardation for $\sigma = 0.0$, Figure 3) in which the spread in the particle velocity distribution is unchanged (Figure 5 (top)).

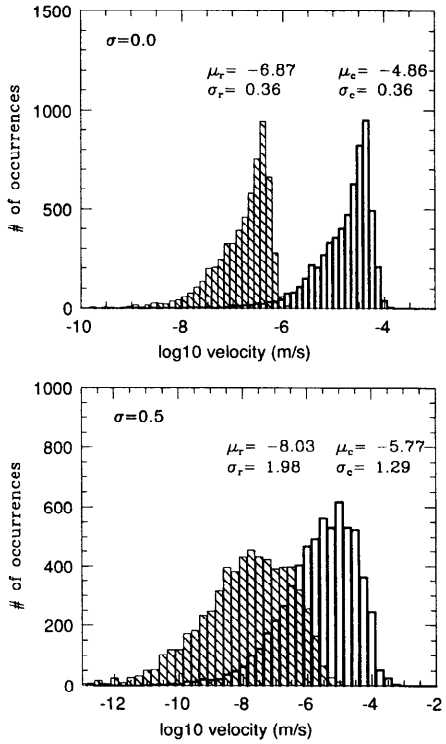

Figure 5. Histograms of the particle velocities in all fracture segments observed in the conservative run (open bars) and retardation run (hatched bars) for a single realization of scenario 1 with (top) σ equal to 0.0 and (bottom) σ equal to 0.5.

This enhanced dispersion in the retarded solute plume due to a coupling of local retardation and local fluid velocities is not limited to a fractured medium. Stochastic analyses of reactive solute movement in a heterogeneous porous medium have shown that a negative cross correlation between the pore water velocity and the local retardation factor may produce enhanced dispersion of the retarded solute plume [e.g., *Garabedian et al.*, 1988; *Valocchi*, 1989; *Bellin et al.*, 1993; *Bosma et al.*, 1993]. It should be kept in mind, however, that our results are not directly comparable to the above studies, which all assume a correlation between the two random fields of sorption coefficients (or retardation factors) and hydraulic conductivity. In the K_a approach for a fractured medium the fluid velocity and retardation factor in a single fracture are related via the fracture aperture. Yet, the overall nature of this relationship is more complicated than a simple negative cross correlation. The fluid velocities are also influenced by the local head gradients which in turn depend on the network geometry as well as the boundary conditions. Hence the solution to the flow problem has a direct bearing on the nature of the relationship between fluid velocity and retardation.

Bellin et al. [1993] further suggested that chemical heterogeneity has a much greater effect on longitudinal spreading than on transverse spreading of the retarded solute plume in a heterogeneous porous medium. A preliminary analysis of the spatial moments in scenarios 1 and 2 suggests that this trend may also exist in a fractured medium (e.g., compare spatial moments in Figure 4). A more detailed analysis is required to confirm this hypothesis. In this context it needs

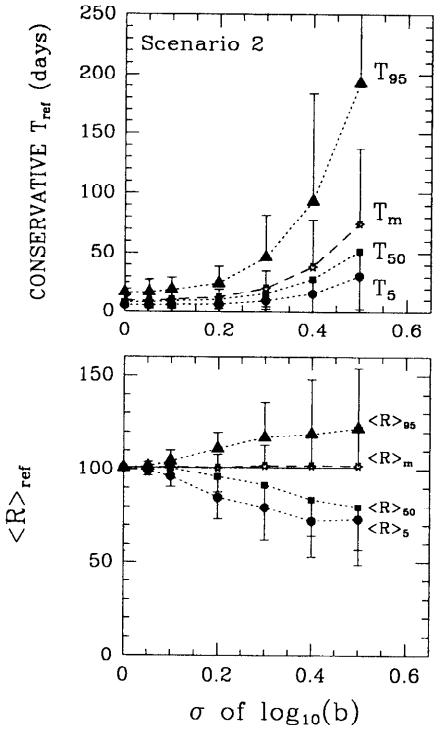

Figure 6. Transport behavior in the sparse network of scenario 2. The two fracture sets have a common aperture distribution (b_m = 80 μm). Shown are the average values for (top) conservative arrival times T_{ref} and (bottom) retardation factors $\langle R \rangle_{ref}$. The standard deviation of these estimates is indicated by the one-sided error bars. The geometric estimates of $\langle R \rangle$ in scenario 2 is equal to 101 (solid line).

to be emphasized that the spatial heterogeneity in retardation in our fracture networks is a result of the physical heterogeneity (i.e., variable aperture) and not chemical heterogeneity (that is variable K_D or K_a) as assumed by *Bellin et al.* [1993]. The presence of a variable sorption strength (K_a) has not been considered here but would certainly further complicate the process of nonuniform retardation.

How can we describe this nonuniform retardation at the continuum scale? The nonlinear coupling of retardation and fluid velocity prohibits in all but a few special cases the use of a transport equation with a constant retardation factor as postulated in (17). However, to our knowledge, a rigorous mathematical model that describes the variable retardation observed (e.g., Figures 3 and 4) in a transport equation is currently not available. A pragmatic alternative would be to consider only the retardation of the "advective flux," that is, retardation of the first time moment (or perhaps retardation of the first spatial moment) of the solute plume. The effects of nonuniform retardation for noncentral parts of the solute plume would then be absorbed in the operator describing the "dispersive flux" using a lumped parameter. This approach is essentially pursued when fitting the advection-dispersion model (equation (3)) to breakthrough curves of a sorbing solute without obtaining the dispersion coefficient a priori from a conservative transport experiment (see *Dverstorp et al.* [1992] for such an application to a fracture network). For example, in scenario 1 with σ equal to 0.5, nonuniform retardation results in enhanced dispersion, and a fit of the advection-dispersion equation would yield a greater "effective" dispersion coefficient for the sorbing solute than for the conservative solute.

Although appealing in its simplicity, we do not recommend this modeling approach for conceptual reasons. The use of a single, lumped parameter which would describe the physical as well as chemical processes (sorption) resulting in dispersion introduces ambiguity into the meaning of the dispersion coefficient. The dispersion coefficient would no longer be solely determined by the hydromechanics of the medium (such as dispersivity) but it would also depend on the sorption strength of any given solute. From a pragmatic point of view this would imply that tracer tests would have to be run for every sorbing solute of interest to determine its "effective" dispersion coefficient. In our opinion, it is preferable to find a model formulation for reactive transport in which each parameter is defined as much as possible by a unique physical or chemical process. Our analysis of the influence of fracture network parameters on nonuniform retardation, discussed in the remainder of this paper, may help to develop a continuum model that accounts explicitly for nonuniform retardation.

Influence of Fracture Density on Retardation

In scenario 2 we have reduced the scan line density of both fracture sets to three fractures per meter, that is, half the scan line density of scenario 1 (Table 1), to demonstrate the influence of fracture density on nonuniform retardation. Figure 6 summarizes the transport behavior in this relatively sparse network type. As a result of the reduction in the number of fractures present in the domain, the conservative travel times are generally much greater than in scenario 1 (Figure 6 (top)).

Apart from this expected reduction in the permeability of the fracture system, the overall transport behavior is remarkably similar to that described for scenario 1. Again we observe a growing spread in the conservative arrival times T_{ref} for large σ (Figure 6 (top)). The retardation of the mean arrival time is predicted by the geometric estimate of $\langle R \rangle$ (Figure 6 (bottom)). Note that the value of $\langle R \rangle$ is the same for scenarios 1 and 2 ($\langle R \rangle$ = 101) despite the difference in total numbers of fractures. This behavior follows since $\langle R \rangle$ is governed by the specific surface area $\langle a \rangle$ which should be independent of the total (or relative) number of fractures present in the networks of scenarios 1 and 2 which have a common mean aperture (where $b_m^1 = b_m^2$; see (14)). As observed earlier, the various $\langle R \rangle_{ref}$ deviate from the geometric retardation factor for σ greater than zero (Figure 6 (bottom)).

Despite these similarities the transport behavior in scenarios 1 and 2 differs in two important aspects. First, a reduction in fracture density introduces a larger variability in the estimates for $\langle R \rangle_{ref}$ and particularly for the conservative T_{ref}, as indicated by the larger error bars for the average values of $\langle R \rangle_{ref}$ and T_{ref} (Figure 6). Second, a sparser network reduces the degree of nonuniformity in retardation, especially at larger σ (compare Figures 3 and 6). Both observations are related to the extent of flow channeling that occurs in the respective network geometries.

An increase in σ generally provides more opportunity for flow channeling due to the increased variability in fracture aperture [e.g., *Nordqvist et al.*, 1992; *Dverstorp et al.*, 1992].

However, the continuity and dominance of individual flow channels differ for different fracture densities. Figure 7 shows the flow distribution for representative single realizations of scenario 1 (top) and scenario 2 (bottom) for σ equal to 0.5. The relative thickness of the bar indicates the amount of flow (volumetric flow rate) passing through a hydraulically connected fracture segment. The flow distribution in these two realizations is typical in that the dense and well-connected fracture network develops several discontinuous flow channels throughout the domain (Figure 7 (top)). In contrast, the sparse and poorly connected fracture network develops one or two dominant and rather continuous flow channels across the flow domain (Figure 7 (bottom)).

This difference in the type of flow channeling has implications for both conservative and reactive transport. In a sparse network the extent of a dominant flow channel and its exact position with respect to the source area are crucial for the conservative transport times. Good access of the source area to the dominant channel will result in fast travel times with little dispersion of the conservative BTC; poor access will result in long travel times and a conservative BTC with a very long tail. When averaging over many Monte Carlo realizations, this uncertainty in the exact position of the dominant flow channel translates into large standard deviations of the average values of T_{ref} (Figure 6 (top)).

Reactive transport is affected similarly by the dominant flow channels developing in a sparse network. Transport of sorbing solutes in such a channel results in less opportunity for biased sampling of fracture apertures. Slow particles as well as fast particles will use this flow path for much of their travel across the domain. As a result, at the scale of individual fractures they sample a similar suite of surface area–to-volume ratios, and thus the retardation factors of the various reference mass fractions are similar as well. Typically, a good connection of the source area to a dominant flow channel will result in low $\langle R \rangle_{\text{ref}}$ with little nonuniformity, whereas a poor connection to a dominant flow channel (or the absence of the continuous flow channel) will give rise to a greater spread of $\langle R \rangle_{\text{ref}}$. The overall effect on retardation at the plume scale is a reduction in the spread of $\langle R \rangle_{\text{ref}}$ albeit with higher variability in the average values of $\langle R \rangle_{\text{ref}}$ (Figure 6 (bottom)).

In contrast, in a dense network with discontinuous flow channels the solute plume disperses more widely into the network, sampling many more fractures. The discontinuous flow channels are only of local importance in focusing flow and transport. The resulting wider spreading of the solute plume and sampling of many more fractures (with different surface area–to-volume ratios) results in a higher degree of nonuniformity in retardation at the plume scale. In a dense network the exact position of the (discontinuous) flow channels with respect to the source area is not crucial, and estimates of $\langle R \rangle_{\text{ref}}$ and T_{ref} are less variable.

We emphasize again that the reduction in fracture density and the resulting tendency for extended flow channels did not cause a general lowering in retardation of the plume. This result appears at first to contradict findings by *Dverstorp et al.* [1992] obtained in sparse fracture networks using numerical migration experiments. They observed that retardation of the center of mass (T_{50}) was on average a factor of 2 lower than expected based on the geometric estimate of specific surface area. From this, the authors concluded that flow channeling reduces the specific surface area. However,

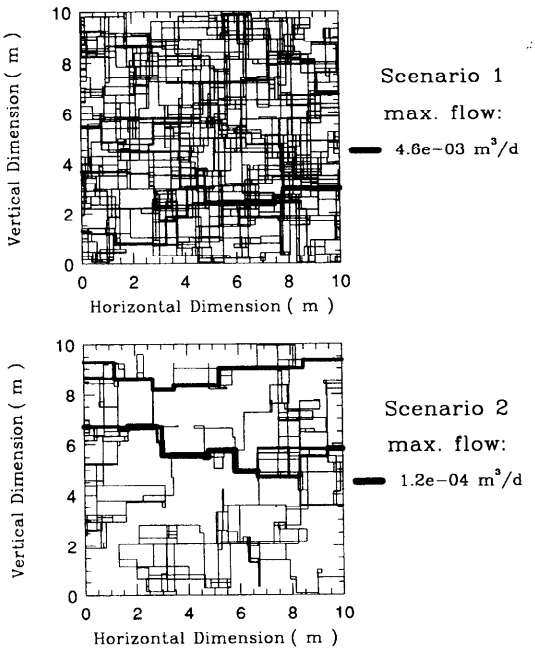

Figure 7. Flow distribution for single realizations of (top) the dense network of scenario 1 and (bottom) the sparse network of scenario 2 for σ equal to 0.5. The relative thickness of the bar indicates the amount of flow (volumetric flow rate) passing through the fracture segment.

Dverstorp et al. failed to acknowledge the nonuniform character of retardation. It is conceivable that the observed reduction in retardation is due entirely to nonuniform retardation, that is, a lower retardation for the center of mass relative to the mean arrival time. According to our results, significant channeling of flow and transport does not, averaged over many Monte Carlo realizations, reduce the retardation of any segment of the solute plume. Instead, the major effect of strong channeling is to increase the variability in $\langle R \rangle_{\text{ref}}$ for a given network description.

The large variability observed in the (conservative and reactive) transport behavior in the sparse network suggests that the domain size of 10 m by 10 m is below the scale of a representative elementary volume (REV) for such a low fracture density (if this REV exists at all). We have not studied larger domain sizes for scenario 2. Nevertheless, it is reasonable to conclude that a decrease in fracture density generally reduces the degree of nonuniformity in retardation. However, there is a greater uncertainty attached in estimating retardation of any segment of the plume.

Two Orthogonal Fracture Sets With Differing Mean Aperture

In scenarios 3 and 4 we study retardation in an orthogonal fracture network consisting of one fracture set with wide fractures (b_m = 80 μm) and a second set with relatively narrow fractures (b_m = 20 μm). Here the orientation of the network with respect to the mean hydraulic gradient has an effect on retardation. Figure 8 shows the retardation behavior for the two scenarios. Note that the only difference between scenarios 3 and 4 is a change in orientation of the entire network by 90° within the flow domain (Table 1).

Three observations summarize the retardation response in

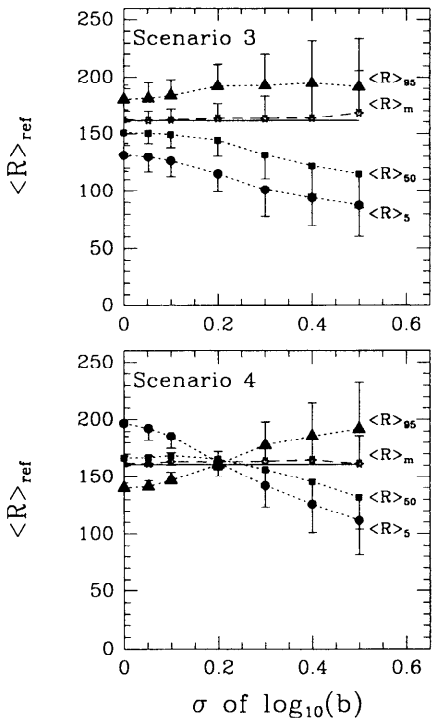

Figure 8. Transport behavior in the dense network of (top) scenario 3 and (bottom) scenario 4. The two fracture sets have differing aperture distributions (b_m^1 = 80 μm and b_m^2 = 20 μm). Shown are the average values of the various retardation factors $\langle R \rangle_{\text{ref}}$. The standard deviation of these estimates is indicated by the one-sided error bars. Scenarios 3 and 4 differ only in their orientation with respect to the mean hydraulic gradient; hence the geometric estimate of $\langle R \rangle$ is equal ($\langle R \rangle$ = 161) in both scenarios (solid lines).

a network where the fracture sets do not have a common aperture distribution. First, the observed retardation factors $\langle R \rangle_{\text{ref}}$ in both scenarios are not equal for the case of two constant aperture values in the respective sets ($\sigma = 0$; Figure 8). This behavior confirms our earlier contention that retardation is only uniform in a network where all fractures have the same aperture value.

Second, retardation of the mean arrival time, $\langle R \rangle_m$, is again described accurately by the geometric retardation factor for both orientations of the fracture network (Figure 8). The geometric estimate of $\langle R \rangle$ in this network (here $\langle R \rangle$ = 161) is greater than in scenario 1 ($\langle R \rangle$ = 101) because the specific surface area in scenarios 3 and 4 is greater due to the smaller mean aperture of the second set (see (16)). By definition, the geometric $\langle R \rangle$ is independent of the orientation of the mean hydraulic gradient to the network and hence is equal in scenarios 3 and 4. The good agreement of this geometric $\langle R \rangle$ and $\langle R \rangle_m$ demonstrates that for these two orientations of the hydraulic gradient, the retardation of the mean arrival time is controlled by the specific surface area of the network. We will show below that $\langle R \rangle_m$ agrees with the geometric $\langle R \rangle$ for any orientation of the fracture network relative to the mean hydraulic gradient.

Third, the difference in the various $\langle R \rangle_{\text{ref}}$ for a given scenario is not only a function of σ but also depends on the orientation of the network relative to the mean hydraulic gradient. In scenario 3, where the fracture set with the larger b_m is oriented in the direction of the mean hydraulic gradient, the degree of nonuniformity increases as a function of σ (Figure 8 (top)). The geometric $\langle R \rangle$ systematically overestimates $\langle R \rangle_{\text{ref}}$ for reference breakthrough fractions ahead of T_m and underestimates $\langle R \rangle_{\text{ref}}$ for reference breakthrough fractions arriving later than T_m (Figure 8 (top)). This behavior is a result of preferential travel of fast particles in wide fractures as discussed for the case of scenario 1. Here the nonuniformity in retardation is more pronounced since the range of fracture apertures is greater (note the change in the scale of the $\langle R \rangle_{\text{ref}}$ axis between Figures 3 (bottom) and 8).

In scenario 4, when the fracture set with the smaller b_m is aligned with the direction of the mean hydraulic gradient, the observed $\langle R \rangle_{\text{ref}}$ fall above and below the geometric $\langle R \rangle$ when considered over the entire range of σ (Figure 8 (bottom)). For small σ the geometric $\langle R \rangle$ underestimates the $\langle R \rangle_{\text{ref}}$ for reference breakthrough fractions ahead of T_{ref} and overestimates $\langle R \rangle_{\text{ref}}$ for reference breakthrough fractions behind T_{ref} (Figure 8 (bottom)). This pattern is gradually reversed as σ increases. The value of σ equal to ~0.2 represents a crossover point at which the four $\langle R \rangle_{\text{ref}}$ are equal.

But what process causes the early breakthrough fractions to be retarded more than the late breakthrough fractions for small σ in scenario 4? This observation is not intuitive and is "forced" by the orientation of the two fracture sets with respect to the mean head gradient. Consider the case of two fracture sets with constant but differing apertures (b_1 = 20 μm and b_2 = 80 μm for $\sigma = 0$). In this configuration, fluid velocities are often greater in the narrow (horizontal) fractures as the influence of the small cross-sectional area (aperture) is more than compensated for by high local head gradients. Similarly, fluid velocities are often smaller in the wider (vertical) fractures due to the small local head gradients. As a result, fast particles will have spent the majority of their (relatively direct) travel path across the domain in horizontal fractures with high retardation. In contrast, slow particles use a more circuituous path involving many more vertical fractures and thus experiencing relatively less retardation. With an increase in the variability of fracture aperture in both sets (larger σ) the difference between wide fractures in one set and narrow fractures in the other set becomes less distinct. At some point (here $\sigma > \sim 0.2$) there are a sufficient number of wide fractures in the horizontal set and narrow fractures in the vertical set so that the fastest particles again travel mostly in wide, horizontal fractures experiencing the lowest retardation.

Note that the unusual form of nonuniform retardation (early breakthrough fractions are retarded more than the late breakthrough fractions) for small σ in scenario 4 implies a reduced dispersion of the retarded solute plume relative to a conservative solute plume. Such a reduction in plume spreading has also been observed in a heterogeneous porous medium for the case of a positively correlated sorption coefficient K_D and hydraulic conductivity [*Bosma et al.*, 1993]. The reason for this reduced dispersion is essentially the same in both fractured and (heterogeneous) porous media, namely, a positive correlation of the local retardation factor and the local fluid velocity. However, the underlying cause for this correlation is physical heterogeneity in the case of the fracture network (variable aperture) and chemical heterogeneity (variable K_D) in the case of a heterogeneous porous medium. This leads to different retardation behavior in response to a change in the physical heterogeneity of each

system. For example, an increase in aperture variability (increase in σ) in scenario 4 produces once again enhanced dispersion of the retarded solute plume indicative of a negative correlation between local retardation factors and local fluid velocities. This change in correlation structure between local retardation and fluid velocity as a function of physical heterogeneity is perhaps unique to a fractured medium.

The different retardation response in scenarios 3 and 4 demonstrates the directional dependence of retardation for various segments of the plume. Therefore retardation at the plume scale has to be considered anisotropic in networks in which the mean fracture aperture differs between two (or more) fracture sets. Given the orientation of the network in these two scenarios (0° and 90° angle from the direction of the mean hydraulic gradient), one might expect that these results represent the maximum possible range of $\langle R \rangle_{ref}$ due to rotation of the network alone. In order to test this hypothesis, two fracture networks (σ = 0.0 and 0.5) of the same network geometry as in scenarios 3 and 4 were rotated in increments of 15° through the flow field using identical boundary conditions as shown in Figure 1. For each orientation, 250 Monte Carlo realizations were used to determine average values of $\langle R \rangle_{ref}$.

The four $\langle R \rangle_{ref}$ determined in these simulations are plotted in polar coordinates, where the angle represents the degrees of rotation of the network and the radius is given by the respective $\langle R \rangle_{ref}$ (Figure 9). Figure 9 (top) shows results for σ = 0.0, while Figure 9 (bottom) is for σ = 0.5. In this presentation the four $\langle R \rangle_{ref}$ for scenario 3 (α_1 = 0°) plot on the x axis and the $\langle R \rangle_{ref}$ for scenario 4 (α_1 = 90°) plot on the y axis. These two orientations are referred to as the principal orientations of the network with respect to retardation. Similarly, the $\langle R \rangle_{ref}$ measured in those two orientations are defined as the principal retardation factors for the respective reference point. The simulation results show that these principal retardation factors indeed represent the maximum range for any given $\langle R \rangle_{ref}$ (Figure 9). The $\langle R \rangle_{ref}$ observed for the intermediate orientations are predicted well by a retardation ellipse using the observed principal retardation factors as minor and major axes.

We have studied only orientations in the range of 0° to 90°. However, retardation factors are symmetrical to both principal orientations due to the symmetry in network geometry and the flow domain. To indicate this symmetry, the retardation ellipses have been drawn for the entire range of α (0°–360°). The good fit of these empirical retardation ellipses indicates that the influence of network orientation on retardation is systematic and predictable.

No-flow boundary conditions were used for the top and bottom boundaries in our analysis to ensure that sufficient particles exit at the downgradient boundary. This procedure could potentially introduce artificial flow and transport behavior ("wall effects"). To test for such boundary effects, transport simulations were also performed for the two principal orientations in flow domains 10 × 20 and 10 × 30, that is twice and 3 times the width of the flow domain shown in Figure 1. No significant differences were found for the various $\langle R \rangle_{ref}$, suggesting that the observed anisotropy in retardation is not influenced significantly by artificial boundary effects.

The retardation ellipses serve to illustrate both the nonuniformity (different values for $\langle R \rangle_{ref}$) and the anisotropy (directional dependence of $\langle R \rangle_{ref}$) of retardation at the plume scale. Both aspects of retardation are governed by the variability in the aperture distribution. Anisotropy in retardation is greatest for σ equal to 0 (Figure 9 (top)). A comparison of the ellipses drawn for $\langle R \rangle_5$ and $\langle R \rangle_{95}$ for this fracture network (σ = 0) shows that the major axis of $\langle R \rangle_5$ corresponds to the minor axis for $\langle R \rangle_{95}$ (Figure 9 (top)). The degree of anisotropy (ratio of major and minor axis) for those two reference points is comparable. For high σ, however, the anisotropic nature of retardation is greatly reduced (Figure 9 (bottom)). In other words, the increased variability in fracture aperture has the effect of decreasing the directional dependence of retardation. This is true in particular for the tail of the plume (see $\langle R \rangle_{95}$ in Figure 9 (bottom)).

The opposite trends are observed for the influence of σ on nonuniformity in retardation. For σ equal to zero the retardation ellipses of the various reference points are relatively close to each other, indicating little nonuniformity (Figure 9 (top)). In fact, retardation is uniform for an intermediate orientation of ~45°. An increase in σ results in greater nonuniformity in retardation, which is apparent in a clear separation of the retardation ellipses so that $\langle R \rangle_5$ is consistently lower and $\langle R \rangle_{95}$ is consistently greater than $\langle R \rangle$ for any orientation of the network within the flow domain (Figure 9 (bottom)).

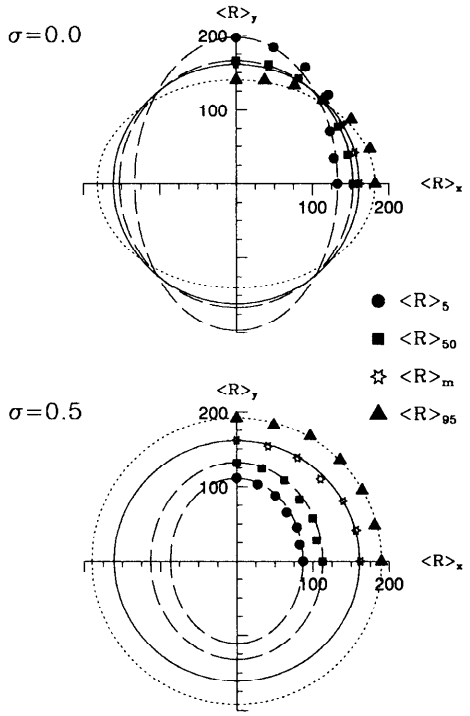

Figure 9. Retardation factors plotted in polar coordinates for a range of network orientations in the flow domain for (top) σ equal to 0.0 and (bottom) σ equal to 0.5. The angle is defined as the angle that the wide fracture set (b_m = 80 μm) spans from the (horizontal) direction of the global hydraulic gradient, and the radius is given by the respective value of $\langle R \rangle_{ref}$. The data points represent the average values of $\langle R \rangle_{ref}$ observed for the four reference mass breakthrough fractions. The data points are obtained by rotating the network of scenario 3 in 15° intervals; the various lines represent retardation ellipses for the four reference points which are constructed based on the principal retardation factors (see text).

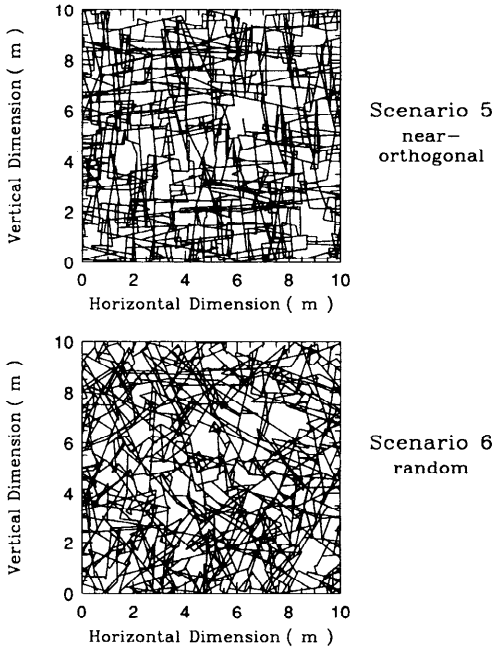

Figure 10. Example realization of (top) a near-orthogonal fracture network in scenario 5 and (bottom) a random network in scenario 6. Only the hydraulically connected network is shown.

Retardation of the mean arrival time is invariant since it is independent of the orientation of the network as well as the spread in fracture aperture. In polar coordinates, $\langle R \rangle_m$ plots as a circle with its radius equal to the geometric estimate of $\langle R \rangle$ for any σ (Figure 9). Note that all $\langle R \rangle_{ref}$ of scenarios 3 and 4 would fall on this circle if retardation was isotropic and uniform.

In theory, knowledge of the principal retardation factors for any given reference breakthrough fraction would be sufficient to predict retardation for any orientation of the network. Unfortunately, an analytical formulation of the principal retardation factors has not yet been found. It is clear, however, that the magnitude of the principal retardation factors is directly related to (1) the aperture distribution (described by b_m and σ) for each fracture set and (2) the network geometry (described by fracture density and fracture orientation). In the next section we address the influence of variability in fracture orientation on the extent of nonuniformity and anisotropy in plume retardation.

Influence of Variability in Fracture Orientation on Retardation

In scenarios 5 and 6 we study retardation in networks in which the orientation of the two fracture sets (with differing mean aperture for the sets) is not strictly orthogonal. Transport was simulated in two network geometries with (1) 10° standard deviation about the two mean (orthogonal) orientations ("near-orthogonal orientation") and (2) 90° standard deviation about the two mean (orthogonal) orientations ("random orientation") for the two fracture sets (Table 1). Figures 10 (top) and 10 (bottom) show example realizations of the networks with near-orthogonal and random orientation, respectively. In scenarios 5 and 6, migration experiments were run only in the two principal orientations (0° and 90°; see Table 1) for σ equal to 0.0 and 0.5. We have interpolated the retardation behavior to all intermediate orientations by drawing retardation ellipses using the principal retardation factors obtained for σ equal to 0.0 and 0.5 (Figures 11 and 12, respectively). The retardation ellipses for the near-orthogonal network plot in the upper half of the diagram (Figures 11 (top) and 12 (top)), and those for the random network plot in the lower half of the diagram (Figures 11 (bottom) and 12 (bottom)).

For the case where all apertures for one set are 80 μm, and for the second set 20 μm (i.e., $\sigma = 0.0$), the near-orthogonal network still shows directional dependence in retardation (Figure 11 (top)). As might be expected, a random fracture network shows no directional dependence in retardation (Figure 11 (bottom)). This gradual loss in anisotropy is accompanied with an increase in the nonuniformity of retardation. The overall spread in the various $\langle R \rangle_{ref}$ is considerably greater for the random network than for the near-orthogonal network (Figure 11).

For a large spread in the aperture distribution the degree of anisotropy in retardation is greatly reduced in the near-orthogonal network (Figure 12 (top)). As a result, retardation is consistently nonuniform for any orientation of the network in the flow field. Similar trends have been described already for the orthogonal network (Figure 9). In the network with no preferred (i.e., random) orientation the degree of nonuniformity also increases with an increase in σ (compare Figures 11 (bottom) and 12 (bottom)).

Based on these results the influence of variability in

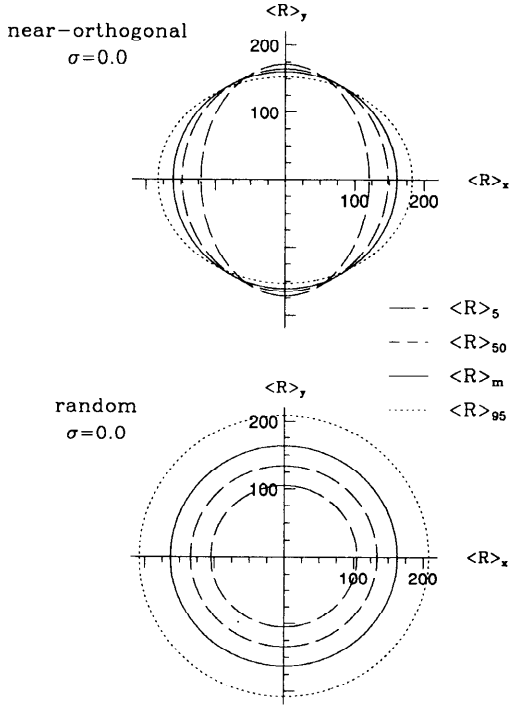

Figure 11. Retardation ellipses for (top) the near-orthogonal network of scenario 5 and (bottom) the random network of scenario 6 for σ equal to 0.0. The ellipses are constructed based on transport simulations with the networks oriented in the two principal orientations (0° and 90°). Retardation ellipses are drawn for the 5%, 50%, mean, and 95% breakthrough fractions.

fracture orientation on retardation can be summarized as follows. The highest degree of anisotropy in retardation can be expected in a strictly orthogonal fracture network composed of two fracture sets with widely differing mean aperture, in particular if the spread in each aperture distribution is small (low σ). Greater variability in the orientation of the fractures for each set weakens the directional dependence of retardation. There is, however, an increase in nonuniformity, that is, the overall spread in the retardation factors for different reference points on the breakthrough curve.

The reason for this complex dependence of retardation on the mean orientation of fracture sets in the flow field (and its variability) is again found in the coupling of fluid velocity and retardation through fracture aperture. For fracture networks with a common mean aperture (scenarios 1 and 2) and those fracture networks with differing mean apertures in each fracture set but no preferred mean orientation of the sets (scenario 6), fluid velocity is directly proportional to b^2 (i.e., the cross-sectional term in the cubic flow equation (20)). For a network in which the fracture sets have differing preferred mean orientation and aperture is nonuniformly distributed, the relationship of fluid velocity and aperture is further complicated by a correlation of local head gradients and fracture aperture. The general nature of this correlation (i.e., positive or negative) is determined by which fracture set is more closely aligned with the mean hydraulic gradient. The strength of this correlation and its influence on retardation are determined by the variability about the preferred orientation, that is, the extent to which the fracture sets are preferentially oriented.

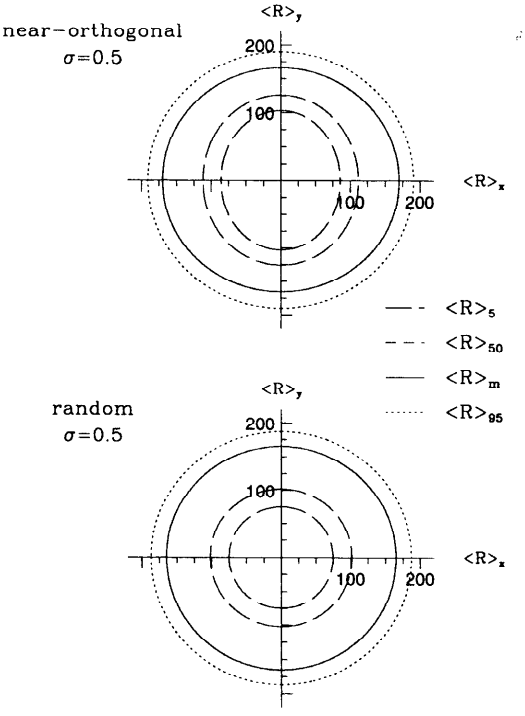

Figure 12. Retardation ellipses for (top) the near-orthogonal network of scenario 5 and (bottom) the random network of scenario 6 for σ equal to 0.5. The ellipses are constructed based on transport simulations with the networks oriented in the two principal orientations (0° and 90°). Retardation ellipses are drawn for the 5%, 50%, mean, and 95% breakthrough fractions.

Limitations of This Study

The applicability of our findings is clearly limited by our assumptions. With respect to the fracture network we have assumed a two-dimensional network of parallel plates. In reality, a fractured medium is composed of fracture planes with rough surfaces in a three-dimensional configuration. However, the mechanisms responsible for nonuniform and anisotropic retardation are expected to be present in a three-dimensional fracture network as well, namely, the nonlinear coupling of fluid velocity and retardation via the fracture aperture (or more precisely the specific surface area) of any given fracture segment.

Direct surface profiling in natural fractures has shown that natural fractures are often rough and partially closed [e.g., *Brown and Scholz*, 1985]. In experimental studies on flow and transport in single fractures, significant channeling has been observed [e.g., *Abelin et al.*, 1985; *Brown*, 1987]. The parallel plate model may not be adequate to describe the channelized movement of fluid and solutes in such rough, partially closed fractures. *Moreno et al.* [1988] conceptualized the fracture plane as a field of variable fracture apertures with a spatial correlation length. Using numerical migration experiments, they observed channeling phenomena comparable to those observed in experimental studies. *Moreno et al.* [1988] also found that the retardation factor for this variable aperture fracture could be determined from the retardation equation (2) with the use of the mean aperture of the fracture. This result is consistent with our findings for retardation at the network scale. Moreno et al. did not comment on any nonuniformity in the retardation response. Based on our results we anticipate that a variability in local fracture aperture (within a single fracture plane) would also lead to nonuniform retardation even at the scale of a single fracture.

At the network scale the fracture density and the mean orientation of these rough fracture planes in three dimensions should determine to what extent this nonuniformity in retardation at the single fracture scale translates into nonuniformity and anisotropy at the fracture network scale. The general trends presented earlier regarding the influence of fracture density and variability in fracture orientation on retardation in two dimensions should in principle apply to three-dimensional networks of these rough (variable aperture) fractures as well.

Perhaps the most important assumption in the retardation approach presented here is the dependence of retardation on the surface area–to-volume ratio for a single fracture (see (1)). This assumption has been tested, for example, by Vandergraaf and coworkers, who compared surface retardation factors determined from tracer BTCs in machined and natural fractures in granite to those calculated from K_a values determined from static sorption experiments using rock coupons. For migration experiments in machined fractures with residence times of the order of days, retardation factors were in good agreement with those calculated from static K_a values [*Vandergraaf et al.*, 1988]. In another laboratory experiment, *Vandergraaf and Drew* [1991] determined a surface retardation factor for cesium in a natural fracture (0.9 m by 0.9 m) in a block of granite. The observed surface retardation factor (based on retardation of the 50% mass breakthrough fraction) was approximately half of that

expected from the static K_a value. The observed differences in $\langle R \rangle_{50}$ and $\langle R \rangle$ could have resulted from nonuniform retardation due to the roughness of the fracture plane. Unfortunately, retardation of the mean arrival time was not reported. These laboratory results are generally encouraging and suggest that the retardation equation (2) for a single fracture may be applicable.

The retardation equation (2) for a single fracture, as well as its counterpart for a fractured medium (11), assumes that the sorption reaction is instantaneous, that is, that sorption rates are much faster than transport rates. This assumption is commonly referred to as the local equilibrium assumption [e.g., *Brusseau and Rao*, 1989]. For many sorbing solutes this assumption is not strictly valid. Static sorption experiments indicate an increase in K_a values as a function of the time allowed for partitioning [e.g., *Vandergraaf and Drew*, 1991]. As a result, the amount of retardation is often strongly affected by the residence time in the fracture [*Vandergraaf et al.*, 1988]. We are currently investigating under which transport conditions the local equilibrium assumption can be invoked for surface sorption in a single fracture. The parameters of interest here are the sorption rates, the rates of advection and diffusion within the open fracture, and the transport distances involved.

It should be emphasized again that we have considered only surface sorption onto the rock walls. Numerous studies have shown that retardation of a sorbing solute due to matrix diffusion and matrix sorption is potentially significant [e.g., *Neretnieks et al.*, 1982; *Sudicky and McLaren*, 1992; *Maloszewski and Zuber*, 1993]. Matrix sorption has a similar effect on the retardation of the solute plume as has surface sorption in most fracture networks, namely, an increase in dispersion of the sorbing solute plume relative to a conservative solute plume. It may be difficult to distinguish between those two mechanism based on the comparison of conservative and reactive BTCs in a real tracer experiment.

Conclusions

Numerical migration experiments have been performed to study retardation of reactive solutes due to surface sorption in relatively dense two-dimensional fracture networks composed of two fracture sets. The fractures are approximated by parallel plates, and retardation in a single fracture is assumed to vary with the surface area–to-volume ratio of the fracture.

Given these assumptions, retardation at the plume scale is a nonuniform and anisotropic process. Different segments of the plume, or equivalently different breakthrough fractions at a downstream boundary, are retarded to a different degree. The mean arrival time is the only breakthrough fraction that is consistently described by a uniform, isotropic retardation factor which is based on the specific surface area of the network. The degree to which various breakthrough fractions are retarded varies as a function of the orientation of the mean hydraulic gradient relative to the orientation of the fracture sets. This variation can be described in the form of a retardation ellipse.

The degree of nonuniformity and anisotropy in the retardation factor is controlled largely by the difference in the mean apertures of each fracture set, the standard deviation in fracture aperture, and the network geometry (fracture density and fracture orientation). A larger variability in fracture aperture, or in the orientation of fractures within each set, promotes nonuniform retardation while reducing the degree of anisotropy in the retardation factor. Dense fracture networks are more likely to exhibit nonuniform retardation at the plume scale than are sparse networks. The complex retardation behavior is a result of the nonlinear coupling of fluid velocities and retardation via fracture aperture.

Our results suggest that a transport model based on the conventional advection-dispersion equation, using a uniform retardation factor, may be conceptually incorrect, even for a dense fracture network. While the effects of nonuniform retardation modify the dispersive flux in a way that could be described by "effective" dispersion coefficients, it is our opinion that a model formulation is needed that clearly separates chemical effects from those due to hydrodynamic dispersion. One alternative approach to model the process of retardation may be the stochastic continuum approach to transport developed by *Schwartz and Smith* [1988]. In this approach, transport is modeled by repeatedly sampling from velocity distributions uniquely defined for different orientations of solute movements. A consideration of retardation would involve modifying these velocity distributions based on discrete network simulations such as discussed in this paper. In this way the nonuniform and anisotropic nature of retardation at the network scale is accounted for in the model.

Acknowledgments. We thank Roger Beckie and Tom Clemo for the many discussions which have been helpful in formulating our ideas. This research has been supported by a grant from the Natural Science and Engineering Research Council of Canada (NSERC).

References

Abelin, H., I. Neretnieks, S. Tunbrant, and L. Moreno, Final report of the migration in a single fracture—Experimental results and evaluation, *Rep. IR 85-03*, Stripa Proj., Stockholm, 1985.

Bear, J., *The Dynamics of Fluids in Porous Media*, 764 pp., Elsevier, New York, 1972.

Bellin, A., A. Rinaldo, W. J. P. Bosma, S. E. A. T. M. van der Zee, and Y. Rubin, Linear equilibrium adsorbing solute transport in physically and chemically heterogeneous porous formations, 1, Analytical solutions, *Water Resour. Res.*, *29*, 4019–4030, 1993.

Bosma, W. J. P., A. Bellin, S. E. A. T. M. van der Zee, and A. Rinaldo, Linear equilibrium adsorbing solute transport in physically and chemically heterogeneous porous formations, 2, Numerical results, *Water Resour. Res.*, *29*, 4031–4043, 1993.

Brown, S. R., Fluid flow through rock joints: The effect of surface roughness, *J. Geophys. Res.*, *92*(B2), 1337–1347, 1987.

Brown, S. R., and C. H. Scholz, Broad bandwidth study of the topography of natural rock surfaces, *J. Geophys. Res.*, *90*(B14), 12,575–12,582, 1985.

Brusseau, M. L., and P. S. C. Rao, Sorption non-ideality during organic contaminant transport in porous media, *Crit. Rev. Environ. Control*, *19*(1), 33–99, 1989.

Burkholder, H. C., Methods and data for predicting nuclide migration in geologic media, paper presented at International Symposium on Management of Wastes from the LWR Fuel Cycle, Denver, Colo., 1976.

Chernyshev, S. N., and W. R. Dearman, *Rock Fractures*, Butterworth-Heinemann, Stoneham, Mass., 1991.

Clemo, T., Dual permeability modeling for fractured media, Ph.D. thesis, Univ. of B. C., Vancouver, 1994.

Cvetkovic, V. D., and A. M. Shapiro, Mass arrival of sorptive solute in heterogeneous porous media, *Water Resour. Res.*, *26*, 2057–2067, 1990.

Dverstorp, B., J. Andersson, and W. Nordqvist, Discrete fracture

network interpretation of field tracer migration in sparsely fractured rock, *Water Resour. Res.*, *28*, 2327–2343, 1992.

Freeze, R. A., and J. A. Cherry, *Groundwater*, 604 pp., Prentice-Hall, Englewood Cliffs, N. J., 1979.

Garabedian, S. P. L., L. Gelhar, and M. A. Celia, Large-scale dispersive transport in aquifers: Field experiments and reactive transport theory, *Rep. 315*, Ralph M. Parsons Lab., Mass. Inst. of Technol., Cambridge, 1988.

Hull, C. H., J. D. Miller, and T. M. Clemo, Laboratory and simulation studies of solute transport in fracture networks, *Water Resour. Res.*, *23*, 1505–1513, 1987.

Maloszewski, P., and A. Zuber, Tracer experiments in fractured rocks: Matrix diffusion and the validity of models, *Water Resour. Res.*, *29*, 2723–2735, 1993.

Moreno, L., Y. W. Tsang, C. F. Tsang, F. V. Hale, and I. Neretnieks, Flow and transport in a single fracture: A stochastic model and its relation to some field observations, *Water Resour. Res.*, *24*, 2033–2048, 1988.

Neretnieks, I., A note on fracture flow mechanisms in the ground, *Water Resour. Res.*, *19*, 363–370, 1983.

Neretnieks, I., T. Eriksen, and P. Tahtinen, Tracer movement in a single fissure in granitic rock: Some experimental results and their interpretation, *Water Resour. Res.*, *18*, 849–858, 1982.

Nordqvist, A. W., Y. W. Tsang, C. F. Tsang, B. Dverstorp, and J. Andersson, A variable aperture fracture network model for flow and transport in fractured rocks, *Water Resour. Res.*, *28*, 1703–1713, 1992.

Raven, K. G., Hydraulic characterization of a small groundwater flow system in fractured monzonite gneiss, *Pap. 30*, Natl. Hydrol. Res. Inst., Environ. Can., Burlington, Ont., 1986.

Schwartz, F. W., and L. Smith, A continuum approach for modeling mass transport in fractured media, *Water Resour. Res.*, *24*, 1360–1372, 1988.

Smith, L., T. Clemo, and M. D. Robertson, New approaches to the simulation of field-scale solute transport in fractured rocks, paper presented at the 5th Canadian/American Conference on Hydrogeology, Natl. Groundwater Assoc., Calgary, Alta., Canada, 1990.

Snow, D. T., The frequency and aperture of fractures in rock, *Int. J. Rock Mech. Miner. Sci.*, *7*, 23–40, 1970.

Sudicky, E. A., and R. G. McLaren, The Laplace transform Galerkin technique for large-scale simulation of mass transport in discretely fractured porous formations, *Water Resour. Res.*, *28*, 499–514, 1992.

Tsang, Y. W., C. F. Tsang, I. Neretnieks, and L. Moreno, Flow and tracer transport in fractured media: A variable aperture channel model and its properties, *Water Resour. Res.*, *24*, 2049–2060, 1988.

Valocchi, A. J., Spatial moment analysis of the transport of kinetically adsorbing solutes through stratified aquifers, *Water Resour. Res.*, *25*, 273–279, 1989.

Vandergraaf, T. T., and D. J. Drew, Laboratory studies of radionuclide transport in fractured crystalline rock, paper presented at 3rd International Symposium on Advanced Nuclear Energy Research, Jpn. At. Energy Res. Inst., Mito City, 1991.

Vandergraaf, T. T., D. M. Grondin, and D. J. Drew, Laboratory radionuclide migration experiments at a scale of one meter, *Mater. Res. Soc. Symp. Proc.*, *112*, 159–168, 1988.

L. Smith and C. Wels, Department of Geological Sciences, 6339 Stores Road, University of British Columbia, Vancouver, British Columbia, Canada V6T 1Z4.

(Received October 25, 1993; revised April 11, 1994; accepted April 19, 1994.)